



## NRC Publications Archive Archives des publications du CNRC

### **Structural and biochemical investigation of PglF from *Campylobacter jejuni* reveals a new mechanism for a member of the short chain dehydrogenase/reductase superfamily**

Riegert, Alexander S.; Thoden, James B.; Schoenhofen, Ian C.; Watson, David C.; Young, N. Martin; Tipton, Peter A.; Holden, Hazel M.

This publication could be one of several versions: author's original, accepted manuscript or the publisher's version. / La version de cette publication peut être l'une des suivantes : la version prépublication de l'auteur, la version acceptée du manuscrit ou la version de l'éditeur.

For the publisher's version, please access the DOI link below. / Pour consulter la version de l'éditeur, utilisez le lien DOI ci-dessous.

#### **Publisher's version / Version de l'éditeur:**

<https://doi.org/10.1021/acs.biochem.7b00910>

*Biochemistry*, 56, 45, pp. 6030-6040, 2017-10-20

#### **NRC Publications Record / Notice d'Archives des publications de CNRC:**

<https://nrc-publications.canada.ca/eng/view/object/?id=1d867b97-0313-428f-bb5f-554a9dbfe14a>

<https://publications-cnrc.canada.ca/fra/voir/objet/?id=1d867b97-0313-428f-bb5f-554a9dbfe14a>

Access and use of this website and the material on it are subject to the Terms and Conditions set forth at

<https://nrc-publications.canada.ca/eng/copyright>

READ THESE TERMS AND CONDITIONS CAREFULLY BEFORE USING THIS WEBSITE.

L'accès à ce site Web et l'utilisation de son contenu sont assujettis aux conditions présentées dans le site

<https://publications-cnrc.canada.ca/fra/droits>

LISEZ CES CONDITIONS ATTENTIVEMENT AVANT D'UTILISER CE SITE WEB.

**Questions?** Contact the NRC Publications Archive team at

PublicationsArchive-ArchivesPublications@nrc-cnrc.gc.ca. If you wish to email the authors directly, please see the first page of the publication for their contact information.

**Vous avez des questions?** Nous pouvons vous aider. Pour communiquer directement avec un auteur, consultez la première page de la revue dans laquelle son article a été publié afin de trouver ses coordonnées. Si vous n'arrivez pas à les repérer, communiquez avec nous à PublicationsArchive-ArchivesPublications@nrc-cnrc.gc.ca.



# Structural and Biochemical Investigation of PglF from *Campylobacter jejuni* Reveals a New Mechanism for a Member of the Short Chain Dehydrogenase/Reductase Superfamily

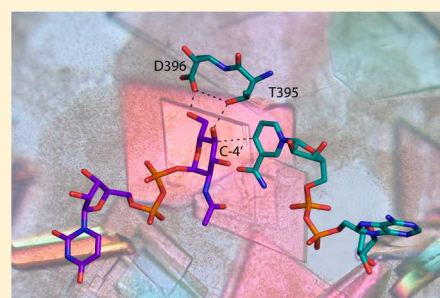
Alexander S. Riegert,<sup>§</sup> James B. Thoden,<sup>§</sup> Ian C. Schoenhofen,<sup>†</sup> David C. Watson,<sup>†</sup> N. Martin Young,<sup>†</sup> Peter A. Tipton,<sup>‡</sup> and Hazel M. Holden<sup>\*,§,Ⓧ</sup>

<sup>§</sup>Department of Biochemistry, University of Wisconsin, Madison, Wisconsin 53706, United States

<sup>†</sup>National Research Council Canada, Human Health Therapeutics, Ottawa, Ontario K1A 0R6, Canada

<sup>‡</sup>Department of Biochemistry, University of Missouri, Columbia, Missouri 65211, United States

**ABSTRACT:** Within recent years it has become apparent that protein glycosylation is not limited to eukaryotes. Indeed, in *Campylobacter jejuni*, a Gram-negative bacterium, more than 60 of its proteins are known to be glycosylated. One of the sugars found in such glycosylated proteins is 2,4-diacetamido-2,4,6-trideoxy- $\alpha$ -D-glucopyranose, hereafter referred to as QuiNAc4NAc. The pathway for its biosynthesis, initiating with UDP-GlcNAc, requires three enzymes referred to as PglF, PglE, and PglD. The focus of this investigation is on PglF, an NAD<sup>+</sup>-dependent sugar 4,6-dehydratase known to belong to the short chain dehydrogenase/reductase (SDR) superfamily. Specifically, PglF catalyzes the first step in the pathway, namely, the dehydration of UDP-GlcNAc to UDP-2-acetamido-2,6-dideoxy- $\alpha$ -D-xylo-hexos-4-ulose. Most members of the SDR superfamily contain a characteristic signature sequence of YXXXX where the conserved tyrosine functions as a catalytic acid or a base. Strikingly, in PglF, this residue is a methionine. Here we describe a detailed structural and functional investigation of PglF from *C. jejuni*. For this investigation five X-ray structures were determined to resolutions of 2.0 Å or better. In addition, kinetic analyses of the wild-type and site-directed variants were performed. On the basis of the data reported herein, a new catalytic mechanism for a SDR superfamily member is proposed that does not require the typically conserved tyrosine residue.



Glycosylation has been well recognized as an important co- or post-translational protein modification in eukaryotes for nearly 80 years. Indeed, the first report of such a modification was published in 1938.<sup>1</sup> Originally thought to be eukaryotic specific, it is now known that such modifications also occur in prokaryotes.<sup>2,3</sup> To date, the best understood prokaryotic N-linked glycosylation pathway is that observed in *Campylobacter jejuni*, a Gram negative organism that is a major culprit in human bacterial gastroenteritis worldwide.<sup>4</sup> Indeed, as first reported in 1999, *C. jejuni* contains an N-linked protein glycosylation pathway, and more than 60 of its proteins are now known to be N-glycosylated by a conserved heptasaccharide.<sup>5,6</sup> The structure of the asparagine-linked heptasaccharide unit, assembled using nucleotide-linked sugars, has been shown to be the following: GalNAc- $\alpha$ 1,4-GalNAc- $\alpha$ 1,4-[Glc $\beta$ 1,3-]GalNAc- $\alpha$ 1,4-GalNAc- $\alpha$ 1,4-GalNAc- $\alpha$ 1,3-diNAcBac- $\beta$ 1 where diNAcBac refers to 2,4-diacetamido-2,4,6-trideoxy- $\alpha$ -D-glucopyranose (also known in the literature as QuiNAc4NAc or N,N'-diacetyl bacillosamine).<sup>7</sup> For this report it will be referred to as QuiNAc4NAc.

The pathway for QuiNAc4NAc production is outlined in Scheme 1.<sup>5</sup> Thus far, the structures and functions of both PglE and PglD have been well characterized.<sup>8–10</sup> The focus of this investigation is on the enzyme PglF, which catalyzes the first step in the pathway, namely, the dehydration of UDP-GlcNAc

to UDP-2-acetamido-2,6-dideoxy- $\alpha$ -D-xylo-hexos-4-ulose. PglF is a NAD<sup>+</sup>-dependent membrane associated protein containing 590 amino acid residues. On the basis of its amino acid sequence, it appears that PglF is composed of three domains: an N-terminal motif containing four transmembrane regions (Met 1–Arg 129), a linker section of unknown function defined by Met 130–Ile 247, and a C-terminal catalytic domain formed by Ser 248–Ile 590.<sup>11</sup>

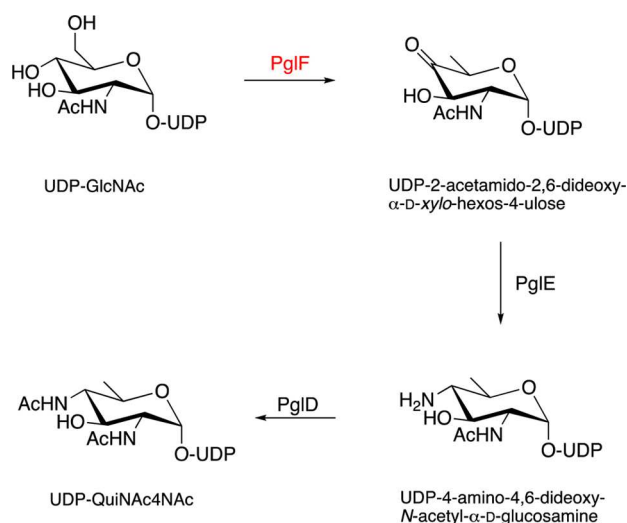
The dehydration step catalyzed by PglF is common to many pathways for the biosynthesis of unusual di- and trideoxy sugars.<sup>12</sup> The enzymes involved in such 4,6-dehydrogenation events are known to belong to the short-chain dehydrogenase/reductase (SDR) superfamily.<sup>13–17</sup> Members of the family are NAD(H)- or NADP(H)-dependent and are involved in a wide range of biological processes including normal and metastatic growth, fertility, and hypertension, among others.<sup>18,19</sup> Despite having limited amino acid sequence identities (15–30%) and varying quaternary structures, members of the SDR superfamily have similar bilobal subunit architectures with their N-terminal regions dominated by a modified Rossmann fold. Two characteristic signature sequences are found in SDR superfamily

**Received:** September 13, 2017

**Revised:** October 19, 2017

**Published:** October 20, 2017

**Scheme 1. Pathway for the Biosynthesis of UDP-QuiNAc4NAc**



members: a YXXXX motif where the conserved tyrosine is thought to serve as a catalytic acid/base and a GXXX[AG]XG motif involved in dinucleotide binding.

During the past 17 years the sugar 4,6-dehydratases have been the focus of numerous structural and biochemical investigations.<sup>20–36</sup> From these studies, and as outlined in Scheme 2, the conserved tyrosine, in its tyrosinate form, is thought to function as the catalytic base that abstracts a proton from the C-4' hydroxyl group of the sugar, while the hydride on C-4' is transferred to a tightly bound NAD<sup>+</sup>. In the second step,

a conserved glutamate (or sometimes a lysine) abstracts a proton from C-5' of the sugar, while a proton from a conserved aspartate is donated to the C-6' hydroxyl moiety thereby leading to the elimination of a water molecule and the formation of a NDP-4-keto-glucose-5,6-ene intermediate. Transfer of the proton from the conserved glutamate back to C-5' and transfer of the hydride from NADH to C-6' yields the final product. Indeed, the mechanism highlighted in Scheme 2 represents the current dogma regarding these intriguing 4,6-dehydratases. Remarkably, in PglF the conserved tyrosine is replaced with a methionine residue, and yet the enzyme is catalytically competent. This change from a tyrosine to a methionine residue was first reported for WbpM from *Pseudomonas aeruginosa*, which is a large membrane bound 4,6-dehydratase that catalyzes the same reaction as PglF.<sup>37</sup> Its three-dimensional structure is unknown, however. The structure of another protein with the tyrosine to methionine replacement was recently reported for CapE from *Staphylococcus aureus*, an enzyme involved in capsular polysaccharide biosynthesis.<sup>35,36</sup>

Herein we describe a detailed structural and functional analysis of PglF from *C. jejuni*. Notably, the closest structural homologue of PglF is FlaA1 from *Helicobacter pylori*, which contains the typical tyrosine residue.<sup>33</sup> On the basis of the data presented, a new catalytic mechanism is put forth for a member of the short-chain dehydrogenase/reductase superfamily that does not require a tyrosine residue to function as a catalytic acid or base.

**Scheme 2. Accepted Mechanism for the Sugar 4,6-Dehydratases**

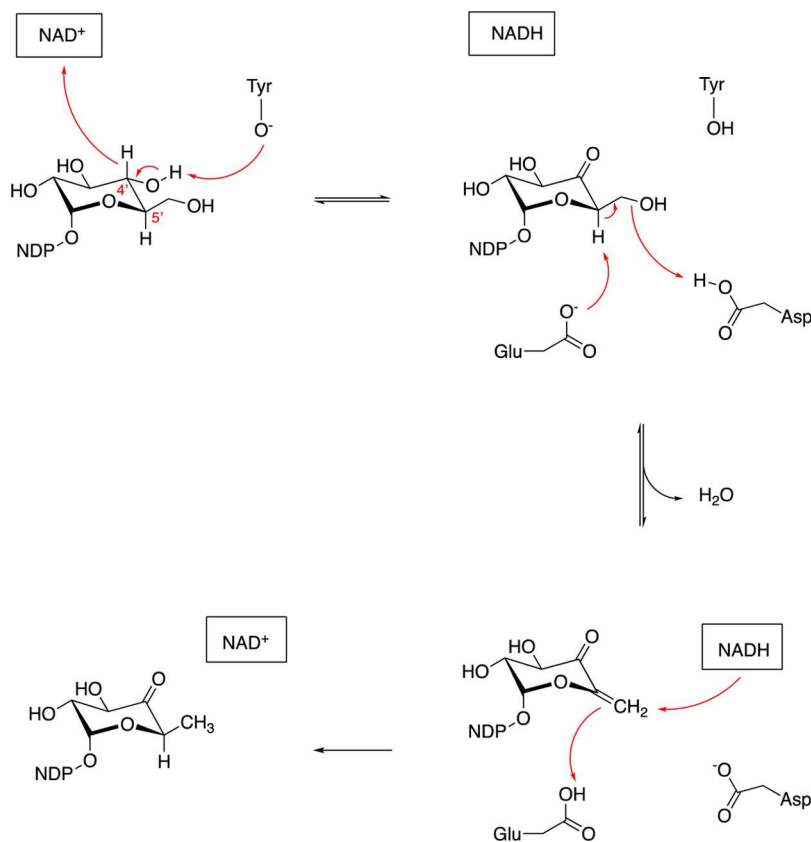


Table 1. X-ray Data Collection Statistics

	wild-type enzyme with NAD(H) and UDP	D396N/K397A variant with NAD(H) and UDP-GlcNAc	T395S variant with NAD(H) and UDP	T395V variant with NAD(H) and UDP	M405Y variant with NAD(H) and UDP
resolution limits	50.0–2.00 (2.10–2.00) <sup>b</sup>	50.0–1.80 (1.90–1.80)	50.0–1.60 (1.63–1.60)	50.0–1.60 (1.66–1.60)	50.0–1.60 (1.66–1.60)
space group	<i>P</i> 2 <sub>1</sub> 2 <sub>1</sub> 2 <sub>1</sub>	<i>P</i> 2 <sub>1</sub> 2 <sub>1</sub> 2 <sub>1</sub>	<i>P</i> 2 <sub>1</sub>	<i>P</i> 2 <sub>1</sub> 2 <sub>1</sub> 2 <sub>1</sub>	<i>P</i> 2 <sub>1</sub> 2 <sub>1</sub> 2 <sub>1</sub>
Unit Cell					
<i>a</i> (Å)	69.1	69.8	59.2	69.2	69.5
<i>b</i> (Å)	107.9	108.5	69.2	108.3	108.3
<i>c</i> (Å)	110.2	109.0	101.5	108.4	109.7
$\beta$ (deg)			100.4		
number of independent reflections	54971 (7076)	74633 (10235)	104005 (5250)	106859 (10499)	103648 (9614)
completeness (%)	97.3 (93.4)	96.4 (89.3)	97.6 (99.7)	99.0 (98.4)	94.7 (88.4)
redundancy	3.7 (2.1)	4.2 (2.0)	4.5 (4.0)	6.8 (5.1)	6.6 (3.8)
avg <i>I</i> /avg $\sigma$ ( <i>I</i> )	13.2 (4.6)	7.7 (2.0)	45.7 (23.6)	58.1 (21.2)	58.3 (10.9)
<i>R</i> <sub>sym</sub> (%) <sup>a</sup>	9.2 (25.3)	9.5 (31.0)	6.3 (10.6)	6.7 (12.1)	6.6 (12.6)

<sup>a</sup> $R_{\text{sym}} = (\sum |I - \bar{I}| / \sum I) \times 100$ . <sup>b</sup>Statistics for the highest resolution bin.

Table 2. Refinement Statistics

	wild-type enzyme with NAD(H) and UDP	D396N/K397A variant with NAD(H) and UDP-GlcNAc	T395S variant with NAD(H) and UDP	T395V variant with NAD(H) and UDP	M405Y variant with NAD(H) and UDP
resolution limits (Å)	50–2.0	50.0–1.8	50.0–1.6	50.0–1.6	50.0–1.6
<i>R</i> -factor <sup>a</sup> (overall)%/no. reflections	19.5/54971	19.4/74633	17.5/104005	16.3/106859	17.0/103648
<i>R</i> -factor (working)%/no. reflections	19.3/52185	19.2/70815	17.3/98833	16.2/96193	16.9/98441
<i>R</i> -factor (free)%/no. reflections	23.7/2728	23.2/3754	20.5/5150	18.5/5315	19.6/5186
number of protein atoms	5400	5397	5326	5401	5371
number of ligands (NAD(H) or UDP or UDP-GlcNAc)	4	4	4	4	4
number of ethylene glycols	1	3	4	5	5
number of sodium ions	2	4	4	8	6
number of water molecules	490	612	697	731	727
<b>average B values</b>					
protein atoms (Å <sup>2</sup> )	17.3	18.1	17.8	15.9	20.9
ligands (Å <sup>2</sup> )	11.7	10.3	12.4	8.6	15.9
solvent (Å <sup>2</sup> )	22.4	26.1	28.9	28.7	32.6
<b>weighted RMS deviations from ideality</b>					
bond lengths (Å)	0.009	0.011	0.011	0.011	0.013
bond angles (deg)	1.7	1.9	1.7	1.7	1.9
general planes (deg)	0.007	0.008	0.008	0.008	0.008
<b>Ramachandran regions (%)<sup>b</sup></b>					
most favored	99.0	98.2	99.6	99.7	99.4
additionally allowed	1.0	1.6	0.4	0.3	0.6
generously allowed		0.1			

<sup>a</sup> $R\text{-factor} = (\sum |F_o - F_c| / \sum |F_o|) \times 100$  where  $F_o$  is the observed structure-factor amplitude and  $F_c$  is the calculated structure-factor amplitude.

<sup>b</sup>Distribution of the Ramachandran angles according to PROCHECK.<sup>42</sup>

## MATERIALS AND METHODS

**Cloning, Expression, and Purification.** A *pglF* gene cloned from *C. jejuni* NCTC11168 served as the starting template for PCR using Platinum Pfx DNA polymerase (Invitrogen). Primers were designed that incorporated NdeI and XhoI restriction sites. The PCR product was digested with NdeI and XhoI and ligated into pET31b. Upon alignment of the *pglF* gene sequence with those of other sugar 4,6-dehydratases, a truncation was incorporated after the transmembrane region and linker domain to create a catalytic globular domain (Ala 244 to the C-terminus). A purification tag

at the C-terminus was also included with the following sequence: AAGFNRIPAAALEHHHHHHH.

The pET31 vector was utilized to transform Rosetta(DE3) *Escherichia coli* cells (Novagen). The cells harboring the pET31b-*pglF* plasmid were cultured in lysogeny broth supplemented with ampicillin (100 mg/L) and chloramphenicol (50 mg/L). The cells were grown with shaking at 37 °C. When the optical density reached 0.8 at 600 nm, the flasks were cooled in an ice water bath, and the cultures were subsequently induced with 1 mM isopropyl  $\beta$ -D-1-thiogalactopyranoside and transferred to a refrigerated shaker at 16 °C where they were allowed to express protein for 18 h after induction.

PglF with the C-terminal histidine tag was purified by nitrilotriacetic acid resin (Qiagen) according to the manufacturer's instructions. Following purification, the protein was dialyzed against 10 mM Tris-HCl and 200 mM NaCl at pH 8.0 and concentrated to 22 mg/mL based on the calculated extinction coefficient of  $1.94 \text{ (mg/mL)}^{-1} \text{ cm}^{-1}$ .

**Site-Directed Mutagenesis.** All site-directed mutant variants of PglF were generated via the QuikChange method of Stratagene. The following protein variants were expressed and purified as described for the wild-type enzyme: D396N/K397A, D396N, T395S, T395V, and M405Y.

**Protein Crystallization and X-ray Structural Analyses.** Crystallization conditions were initially surveyed by the hanging drop method of vapor diffusion using a sparse matrix screen developed in the Holden laboratory. The first experiments were conducted with the wild-type enzyme in complex with 10 mM UDP at room temperature. X-ray diffraction quality crystals appeared as thin plates after 1–2 days and were grown by mixing 1:1 the protein sample at 22 mg/mL with a precipitant solution composed of 22% monomethyl ether poly(ethylene glycol) 5000, 2% 2-methyl-2,4-pentanediol, 10 mM UDP, and 100 mM MES (pH 6.0). Prior to X-ray data collection, the crystals were transferred to solutions composed of 28% monomethyl ether poly(ethylene glycol) 5000, 2% 2-methyl-2,4-pentanediol, 300 mM NaCl, 100 mM MES (pH 6.0), 10 mM UDP, and 15% ethylene glycol. The T395S, T395V, and M405Y mutant variants in the presence of UDP were crystallized under similar conditions to those of the wild-type enzyme.

X-ray diffraction quality crystals of the PglF D396N/K397A variant in the presence of 10 mM UDP-GlcNAc were also grown from hanging drop by mixing 1:1 the protein sample at 20 mg/mL with a precipitant solution composed of 13% monomethyl ether poly(ethylene glycol) 5000 and 100 mM MES (pH 6.0). Prior to X-ray data collection, the crystals were transferred to solutions composed of 24% monomethyl ether poly(ethylene glycol) 5000, 300 mM NaCl, 10 mM UDP-GlcNAc, 100 mM MES (pH 6.0), and 15% ethylene glycol.

X-ray data sets for the PglF wild-type and D396N/K397A mutant variant crystals were collected at 100 K with a Bruker AXS Platinum 135 CCD detector controlled by the Proteum software suite (Bruker AXS Inc.). The X-ray source was Cu  $K\alpha$  radiation from a Rigaku RU200 X-ray generator equipped with Montel optics and operated at 50 kV and 90 mA. These X-ray data were processed with SAINT version 7.06A (Bruker AXS Inc.) and internally scaled with SADABS version 2005/1 (Bruker AXS Inc.). Relevant X-ray data collection statistics are listed in Table 1.

The structure of wild-type PglF was determined via molecular replacement with the software package PHASER<sup>38</sup> and using as a search model the partially refined PglF X-ray coordinates from the laboratory of Dr. Allan Matte. Iterative cycles of model building with COOT<sup>39</sup> and refinement with REFMAC<sup>40</sup> reduced the  $R_{\text{work}}$  and  $R_{\text{free}}$  to 19.3% and 23.7%, respectively, from 50 to 2.0 Å resolution. The structure of the PglF D396N/K397A/UDP-GlcNAc complex was refined in a similar manner. Iterative cycles of model building with COOT and refinement with REFMAC reduced the  $R_{\text{work}}$  and  $R_{\text{free}}$  to 19.2% and 23.2%, respectively, from 50 to 1.80 Å resolution. Relevant refinement statistics are listed in Table 2. Note that noncrystallographic symmetry restraints were never utilized during the model refinements.

X-ray data sets from the T395S, T395V, and M405Y mutant protein crystals were collected at the Structural Biology Center beamline 19-BM at a wavelength of 0.9794 Å (Advanced Photon Source). The X-ray data were processed and scaled with HKL3000.<sup>41</sup> The structures were solved via molecular replacement with the software package PHASER using the wild-type enzyme coordinates as the search model. Relevant refinement statistics are listed in Table 2.

**Kinetic Analyses.** The kinetic constants for the wild-type PglF and all mutant variants were determined via a discontinuous assay using an ÄKTA HPLC system. The reaction rates were determined by coupling PglF with the aminotransferase (PglE) which immediately follows it in the biosynthetic pathway (Scheme 1) and calculating the amount of aminated product (UDP-4-amino-4,6-dideoxy-*N*-acetyl- $\alpha$ -D-glucosamine) formed on the basis of the peak area on the HPLC trace as measured at 262 nm. The area was correlated to concentration via a calibration curve created with standard samples that had been treated in the same manner as the reaction aliquots. The PglE required for the assay was prepared as previously described.<sup>8</sup>

Specifically, the kinetic parameters for the wild-type enzyme with UDP-GlcNAc as a substrate were determined using 2.5 mL reaction mixtures containing 50 mM HEPES (pH 8.0), 1 mM pyridoxal 5'-phosphate, 50 mM sodium glutamate, 1 mg/mL PglE, 0.088  $\mu$ M PglF, and substrate concentrations ranging from 0.1 to 10 mM UDP-GlcNAc. Eight 250  $\mu$ L aliquots were taken at time points over 3.5 min, and the reactions were quenched by the addition of 6  $\mu$ L of 6 M HCl. Subsequently, 200  $\mu$ L of carbon tetrachloride was added, the samples were vigorously mixed and spun at  $14000 \times g$  for 2 min, and 100  $\mu$ L of the aqueous phase was taken for analysis via HPLC. The samples were diluted with 2 mL of water and loaded onto a 1 mL ResQ column. The products were quantified after elution with a 10-column volume gradient from 0 to 725 mM ammonium acetate (pH 6.0).

Kinetic parameters for the M405Y variant with UDP-GlcNAc were determined in a similar manner using 2.5 mL reaction mixtures containing 50 mM HEPES (pH 8.0), 1 mM pyridoxal 5'-phosphate, 50 mM sodium glutamate, 1 mg/mL PglE, 1.3  $\mu$ M PglF, and substrate concentrations ranging from 0.05 to 4 mM UDP-GlcNAc. Eight 200  $\mu$ L aliquots were taken at time points over 10 min, and the reactions were quenched by the addition of 6  $\mu$ L of 6 M HCl.

Kinetic parameters for the T395S variant with UDP-GlcNAc were also determined in a similar manner using 2.5 mL reaction mixtures containing 50 mM HEPES (pH 8.0), 1 mM pyridoxal 5'-phosphate, 50 mM sodium glutamate, 1 mg/mL PglE, 0.10  $\mu$ M PglF, and substrate concentrations ranging from 0.1 to 20 mM UDP-GlcNAc. Eight 200  $\mu$ L aliquots were taken at time points over 10 min, and the reactions were quenched by the addition of 6  $\mu$ L of 6 M HCl.

Using the above assay conditions, no enzymatic activity could be detected for the D396N and T395V variants. Relevant steady state kinetic parameters are listed in Table 3.

**Table 3. Steady State Kinetic Parameters**

enzyme	$K_M$ (mM)	$k_{\text{cat}}$ ( $\text{s}^{-1}$ )	$k_{\text{cat}}/K_M$ ( $\text{M}^{-1} \text{s}^{-1}$ )
wild-type	$0.99 \pm 0.20$	$4.61 \pm 0.35$	$4700 \pm 700$
T395S variant	$2.25 \pm 0.36$	$4.95 \pm 0.56$	$2200 \pm 260$
M405Y variant	$0.20 \pm 0.04$	$0.086 \pm 0.014$	$430 \pm 75$

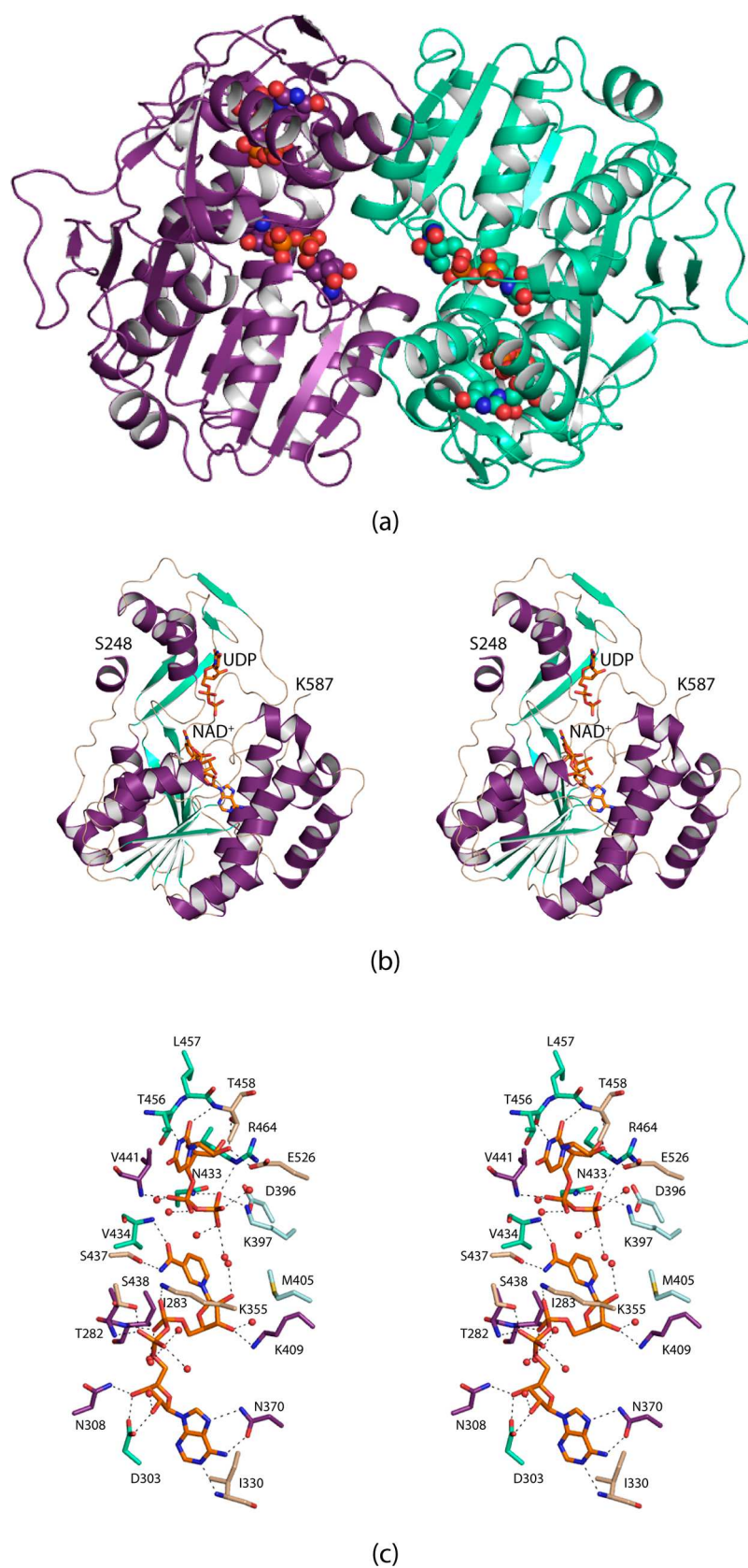


**Figure 1.** Structure of PglF. Shown in (a) is a ribbon representation of the PglF dimer with subunits 1 and 2 depicted in violet and green cyan, respectively. The bound NAD(H) and UDP ligands are drawn in space filling representations. A stereoview of subunit 1 is presented in (b) with the  $\alpha$ -helices displayed in violet and the  $\beta$ -strands colored in green cyan. The bound ligands are drawn in stick representations. A close-up stereoview of the active site for subunit 1 is provided in (c). Water molecules are represented by red spheres. Possible hydrogen bonding interactions, within 3.2 Å, are indicated by the dashed lines. All figures were prepared with PyMOL.<sup>46</sup>

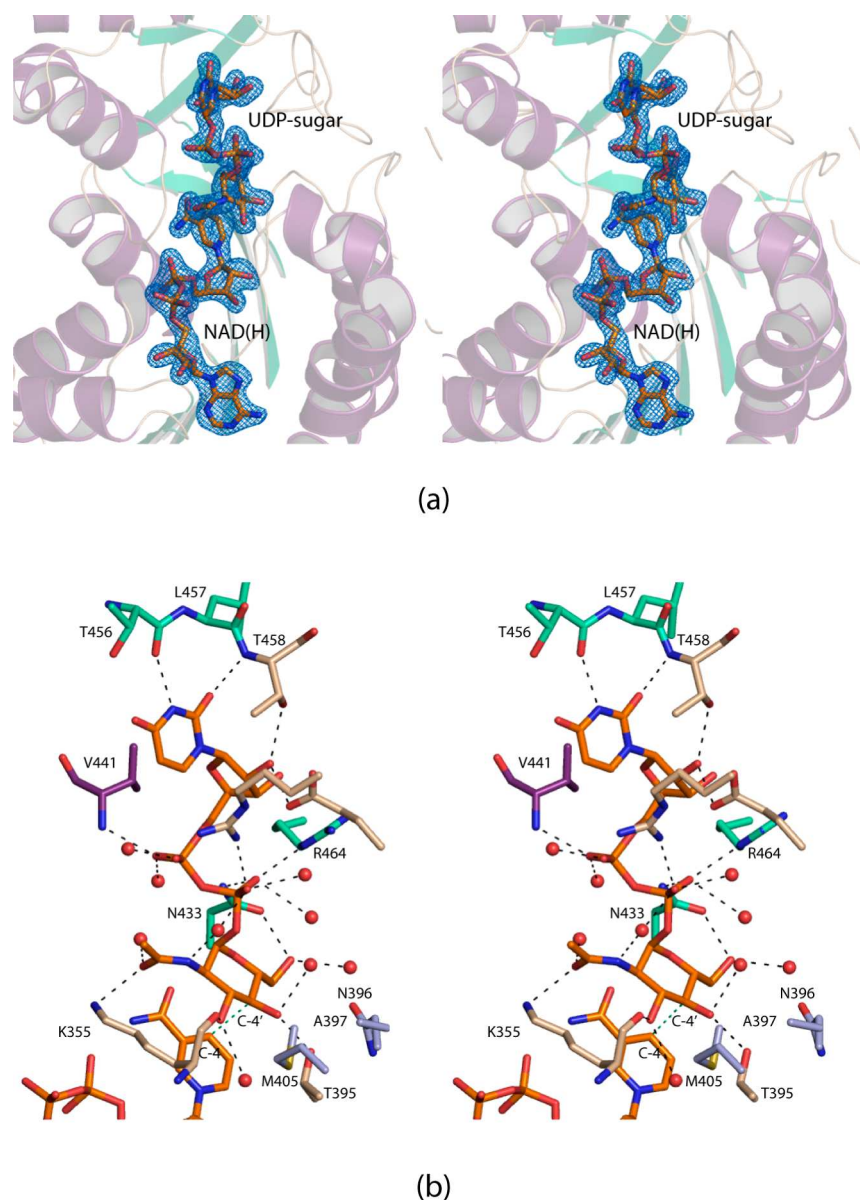


**Figure 2.** Structure of the PglF/(D396N/K397A)/NAD(H)/UDP-GlcNAc complex. The electron densities corresponding to the bound ligands are shown in (a). The electron density map was calculated with  $(F_o - F_c)$  coefficients and contoured at  $3\sigma$ . The ligands were not included in the X-ray coordinate file used to calculate the omit map, and thus there is no model bias. A close-up view of the active site is depicted in (b). Water molecules are displayed as red spheres, and possible hydrogen bonding interactions are indicated by the dashed lines. As indicated by the green line between C-4' of the sugar and C-4 of the nicotinamide ring, the substrate is ideally positioned in the active site for hydride transfer.

Note that the concentration of PglE utilized in the assays ensured that the aminotransferase reaction was not rate-limiting.

Stopped-flow kinetic experiments were performed with a KinTek SF-2001 instrument using absorbance detection with the monochromator set at 340 nm. The mixing chamber was maintained at 25 °C with a circulating water bath. Identical solutions were prepared in H<sub>2</sub>O and in D<sub>2</sub>O. One syringe contained 108  $\mu$ M PglF and the other contained 20 mM UDP-GlcNAc; both solutions were buffered with 50 mM HEPES, pH(D) 8.0, and 150 mM NaCl.

## RESULTS AND DISCUSSION

**Overall Architecture of PglF.** PglF is a membrane bound protein. In order to simplify the structural analysis, various truncation mutant variants were constructed in the linker

region. In most cases, catalytic activity was retained, and the variants expressed well in *E. coli*. Importantly, only those mutant proteins that were truncated near the catalytic domain yielded preliminary crystals. After many trials, the final protein construct utilized in this investigation extended from Ser 248 to Lys 587. Also, the cofactor is referred to as NAD(H) throughout this paper in light of the fact that its exact oxidation state is unknown.

The first structure determined in this investigation was that of the PglF/NAD(H)/UDP ternary complex. The crystals utilized belonged to the space group  $P2_12_12_1$  with two subunits in the asymmetric unit. These two subunits were related by 180° rotation suggesting a dimeric quaternary structure. The model was refined at 2.0 Å resolution to an overall *R*-factor of 19.5%. A ribbon representation of the dimer is presented in Figure 1a. It has overall dimensions of  $\sim 58 \text{ \AA} \times 81 \text{ \AA} \times 63 \text{ \AA}$

and a total buried surface area of 2400 Å<sup>2</sup>. The quaternary structure of PglF, as observed in the asymmetric unit, is decidedly different from that for other dimeric sugar 4,6-dehydratases. Typically, in these enzymes the interface is formed by a four  $\alpha$ -helical bundle with each subunit providing two  $\alpha$ -helical regions.<sup>43</sup> Additionally, the adenosine amino groups of the bound NAD(H) cofactors are separated by ~22 Å. In PglF, the two  $\alpha$ -helical regions required for the formation of the four  $\alpha$ -helical bundle are located nearly on the opposite sides of the subunit–subunit interface. As a consequence, the adenosine amino groups of the bound NAD(H) cofactors in PglF are separated by only ~11 Å. One caveat, however, is that the transmembrane linker was removed from PglF, and thus it is possible that the packing arrangement seen in the crystalline lattice is an artifact. Nevertheless, the total buried surface area as well as the nature of the subunit/subunit interface is suggestive of a dimeric quaternary structure. Furthermore, gel filtration experiments on the protein utilized in this investigation were indicative of a dimer (unpublished data).

The  $\alpha$ -carbons for the two subunits of the PglF dimer superimpose with a root-mean-square deviation of 0.1 Å. Given the close structural correspondence, the following discussion refers only to subunit 1 in the X-ray coordinate file unless otherwise indicated. Shown in Figure 1b is a ribbon representation of the subunit which displays a bilobal type architecture. The polypeptide chain initiates with a short  $\alpha$ -helix followed by random coil. The N-terminal domain responsible for binding NAD(H) is dominated by an eight-stranded parallel  $\beta$ -sheet flanked on each side by three  $\alpha$ -helices. The C-terminal domain that houses the substrate binding site is characterized primarily by two  $\alpha$ -helices and two  $\beta$ -sheets containing two  $\beta$ -strands each.

A close-up stereoview of the active site is displayed in Figure 1c. Both the UDP and NAD(H) ligands are anchored into the active site via numerous hydrogen bonding interactions. Specifically, the uracil ring of UDP lies within 3.2 Å of the carbonyl oxygen and the backbone amide nitrogen of Thr 456 and Thr 458, respectively. The UDP ribose adopts the C2'-*endo* pucker with the C-2 hydroxyl group hydrogen bonding to the side chains of Thr 458 and Glu 526. The side chains of Lys 397, Asn 433, and Arg 464 interact with a  $\beta$ -phosphoryl oxygen of the UDP ligand whereas the backbone amide nitrogen of Val 441 hydrogen bonds to an  $\alpha$ -phosphoryl oxygen. Five water molecules within 3.2 Å surround the UDP ligand. As expected for members of the short chain dehydrogenase/reductase superfamily, the nicotinamide moiety of the NAD(H) adopts the *syn* conformation thereby positioning the B-side of the ring toward the UDP ligand. The side chain of Ser 437 and the amide nitrogen of Val 434 hydrogen bond to the carboxamide group of the nicotinamide ring. Those side chains that play key roles in anchoring the NAD(H) cofactor into the active site cleft include Asp 303, Asn 308, Lys 355, Asn 370, Lys 409, and Ser 438. Additionally, the backbone amide nitrogens of Thr 282, Ile 283, and Ile 330 and six ordered water molecules aid in cofactor positioning. Both Asp 396 and Lys 397 are conserved among some sugar 4,6-dehydratases, but strikingly Met 405 resides in the region normally occupied by a tyrosine residue, which is thought to serve as a catalytic base in these enzymes.

**Active Site Geometry of PglF.** From previous reports on a similar sugar 4,6-dehydratase, it can be speculated that both Asp 396 and Lys 397 in PglF play critical roles in catalysis.<sup>33</sup> Thus, in order to prepare a ternary complex of the enzyme with NAD(H) and its substrate, UDP-GlcNAc, a double site-

directed mutant protein, D396N/K397A, was subsequently prepared. Crystals of this mutant variant with bound NAD(H) and UDP-GlcNAc also belonged to the space group  $P2_12_12_1$  with a dimer in the asymmetric unit. The model was refined at 1.8 Å resolution to an overall *R*-factor of 19.4%. The root-mean-square deviation between the  $\alpha$ -carbons for the wild-type enzyme and the mutant variant superimpose with a root-mean-square deviation of 0.3 Å, thus indicating little structural change upon UDP-sugar binding, at least in the crystalline state. Shown in Figure 2a is the observed electron density corresponding to the bound ligands in subunit 1. As can be seen, the electron density is unambiguous for both the UDP-sugar and the NAD(H) cofactor. The pyranosyl group of the UDP-sugar adopts the <sup>4</sup>C<sub>1</sub> conformation. A stereoview of the PglF ternary complex active site is presented in Figure 2b. Those side chains important for anchoring the pyranosyl group to the protein include Lys 355 and Thr 395. In addition, nine waters surround the bound substrate. Importantly, the sugar C-4' lies within 3.9 Å of the nicotinamide C-4 carbon, and it is also in the proper orientation for hydride transfer.

**Kinetic Analyses of PglF.** Given that the typical tyrosine residue in the sugar 4,6-dehydratases is not found in PglF, the question then arises as to the identity of the catalytic base required to initiate the first half of the reaction outlined in Scheme 2. It is particularly noteworthy that in the wild-type structure, the side chain of Thr 395 is positioned at 3.5 Å from a carboxylate oxygen of Asp 396, and in the ternary complex it is located at 2.8 Å from the sugar C-4' hydroxyl group. It can thus be envisioned that the side chain of Thr 395 might function as a proton shuttle by linking the sugar C-4' hydroxyl group to the side chain of Asp 396, which would ultimately serve as the catalytic base.

To more fully address the roles of the individual amino acids in the activity of PglF, the following site-directed mutant proteins were constructed: T395S, T395V, D396N, and M405Y. Under the assay conditions utilized, no measurable activity was detected for the D396N mutant variant. Because the crystals of the D396N mutant variant were not of high quality, the structure of it will not be reported here.

Mutation at Thr 395 showed an interesting pattern. When changed to a serine, the enzyme retained catalytic activity albeit at a reduced level (Table 3). The major cause for the reduced catalytic efficiency was the increased *K<sub>M</sub>* for the UDP-sugar substrate: 0.99 ± 0.20 mM for the wild-type enzyme versus 2.25 ± 0.36 mM for the T395S variant. Within experimental error, the *k<sub>cat</sub>* values for the two proteins were the same, however (Table 3). Given that Thr 395 is important in positioning the pyranosyl group into the active site, it is not surprising that the *K<sub>M</sub>* would be affected. The loss of the methyl group in substituting a serine for a threonine most likely opens the active site enough to raise the *K<sub>M</sub>* for the UDP-sugar substrate. The three-dimensional structure of the T395S mutant variant was subsequently determined to 1.6 Å resolution, and the model was refined to an overall *R*-factor of 17.5%. The wild-type protein and T395S mutant variant structures are remarkably similar such that their  $\alpha$ -carbons superimpose with a root-mean-square deviation of 0.1 Å. Unlike that observed for the T395S variant, mutation of Thr 395 to a valine residue resulted in a completely inactive protein. To ensure no major structural changes occurred upon this mutation, the structure of the T395V mutant protein was subsequently determined to 1.6 Å resolution (overall *R*-factor of 16.3%). As expected, the structures of the wild-type enzyme

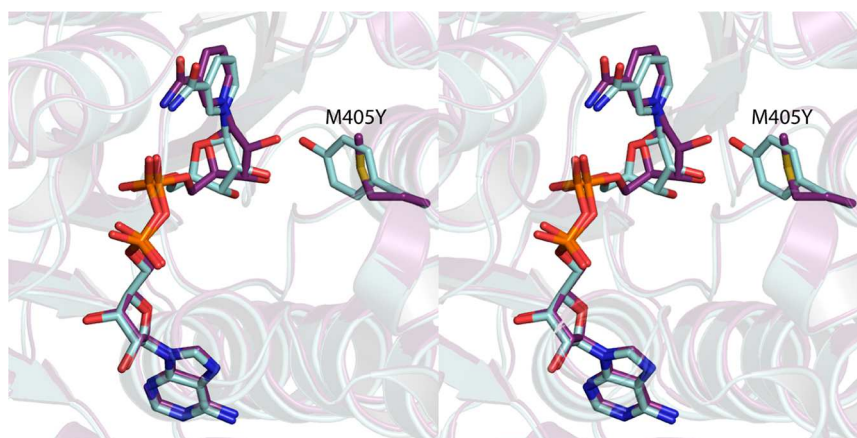
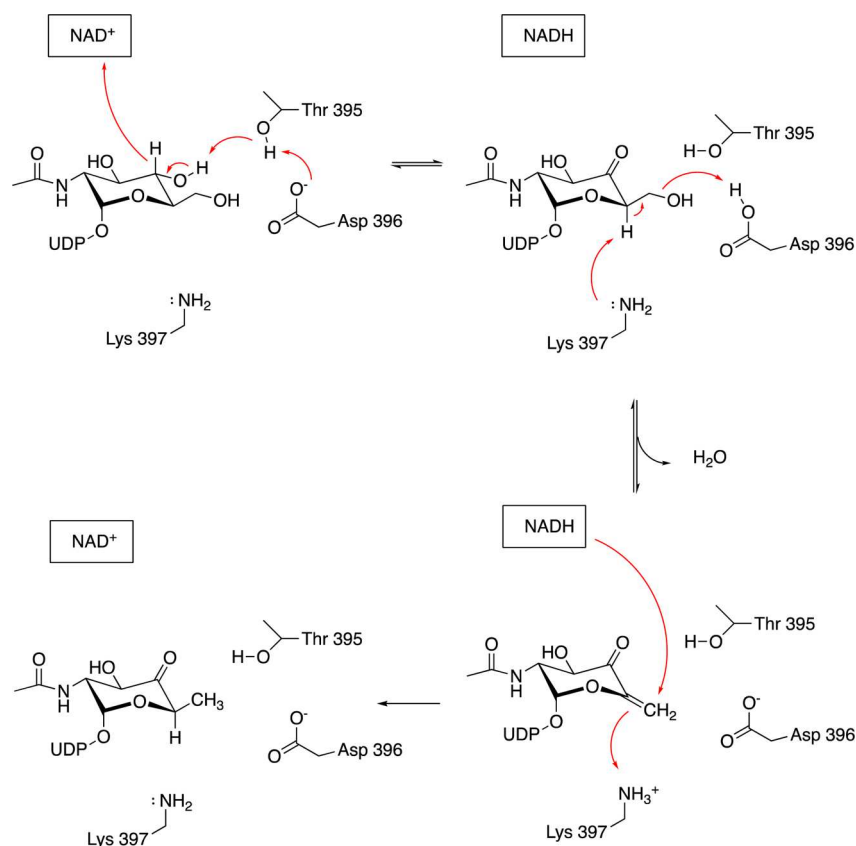


**Figure 3.** Major change that occurs upon substitution of a tyrosine residue for the active site methionine. Shown in stereo are the positions of the NAD(H) cofactors and the side chains in the wild-type (violet) and the M405Y mutant variant (light blue).

### Scheme 3. Proposed Mechanism for the PglF Reaction



and T395V protein variant are nearly identical such that their  $\alpha$ -carbons superimpose with a root-mean-square deviation of 0.2 Å. The above results clearly indicate the importance of a hydroxyl group at position 395 for the PglF reaction mechanism.

We sought additional evidence for a proton-shuttle mechanism from a proton inventory experiment. Hydride transfer to  $\text{NAD}^+$  is concomitant with proton abstraction from the hydroxyl group at C-4'; if this proton removal is mediated by Thr 395, which is itself deprotonated by Asp 396, the formation of NADH would occur with two protons in flight in the transition state. However, the transient increase in absorbance at 340 nm observed in multiturnover experiments

conducted in either protio or deuterio solvent, with enzyme saturated with UDP-GlcNAc, was negligible, equivalent to no more than 0.3% of the enzyme active sites, frustrating our attempt to perform the proton inventory experiment. The absence of NADH accumulation indicates that its formation is rate-limiting in the catalytic cycle.

Given that the typically conserved tyrosine residue in the sugar 4,6-dehydratases is a methionine in PglF, we were curious as to whether the enzyme would retain activity if the methionine was converted to a tyrosine. Thus, the M405Y variant was constructed, and its enzymatic activity assessed. As can be seen in Table 3, the  $K_M$  decreased to  $0.20 \pm 0.04$  mM, whereas the  $k_{\text{cat}}$  was severely reduced to  $0.086 \pm 0.014$  mM.

The structure of the M405Y, determined at 1.6 Å resolution (overall *R*-factor of 17.0%), reveals the largest three-dimensional perturbation among the site-directed mutant proteins that were studied in this investigation. Whereas the  $\alpha$ -carbons for the wild-type enzyme and the M405Y mutant variant superimpose with a root-mean-square deviation of 0.2 Å, the substitution of a tyrosine for a methionine effectively positions the ribose of the NAD(H) more into the active site pocket as shown in Figure 3.

**Catalytic Mechanism of PglF.** On the basis of the observed residues in the active site and the kinetic behavior of the PglF variants that were characterized, a mechanism that does not rely on a tyrosinate is proposed (Scheme 3). The proton transfer that initiates the catalytic cycle is mediated by Thr 395 and Asp 396. The critical roles played by these residues are evident from the fact that the D396N and T395V variants exhibited no detectable catalytic activity. The carboxyl group of Asp 396 is about 4.3 Å from the substrate hydroxyl group that must be deprotonated. This distance is too great for Asp 396 to serve as the general base directly, unless it moves closer to the substrate during the catalytic cycle. However, Thr 395 is positioned to act as an intermediary between the substrate hydroxyl and the carboxylate of Asp 396 (Figure 4).

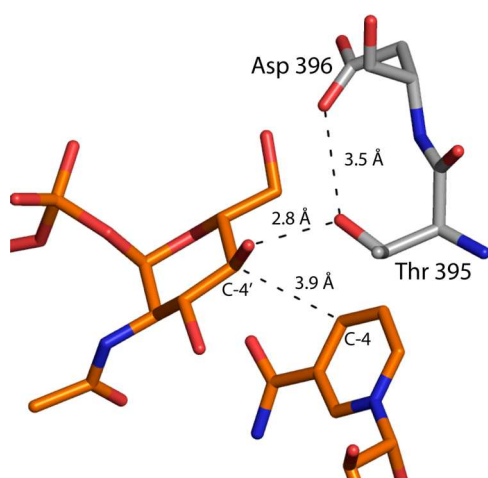


**Figure 4.** Model of the PglF active site before catalysis. The composite illustration was prepared by superimposing the structure of the wild-type PglF with that of the D396N/K397A variant. The positions of the UDP-GlcNAc substrate and the cofactor are derived from the double mutant structure whereas the positions of the side chains of Thr 395 and Asp 396 are based upon the wild-type structure.

Concerted proton transfers between the C-4' hydroxyl, Thr 395, and Asp 396 effect the deprotonation of the substrate and obviate any need for Asp 396 to move. On the basis of the kinetic behavior of the T395S mutant variant, it appears that serine can also act as a bridge between the substrate and Asp 396. After the initial proton transfer, Asp 396 is in the correct position and protonation state to act as a general acid to facilitate dehydration of the intermediate in the next step of the reaction. Lys 397 is positioned to abstract the C-5' proton required to initiate the dehydration. The catalytic cycle closes when NADH delivers a hydride to C-6' and a proton is returned to C-5' by Lys 397. The residues that mediate all the proton transfers that occur are in the same protonation state at the end of the catalytic cycle as they are at the beginning.

Although the sugar 4,6-dehydratases and the sugar C-4' epimerases share little amino acid sequence homology, their

strikingly similar architectures and catalytic mechanisms have caused them to be linked together within the SDR superfamily. The “SYK” catalytic triad in the C-4' epimerases has been studied in detail, and its role in catalysis appears unequivocal.<sup>44,45</sup> Many of the sugar 4,6-dehydratases also have the “SYK” catalytic triad. In some, however, a conserved “SMK” motif has been identified, raising the question of how a methionine residue could substitute for a tyrosine as a general base.<sup>35–37</sup> From the work presented here and in light of basic chemical principles, the methionine does not serve as a catalytic base. Rather it is the combination of Thr 395 and Asp 396 that ultimately removes the proton from the C-4' hydroxyl group. As such, the analogy between the “SMK” and the “SYK” motifs that has been made in the literature is somewhat misleading.<sup>37</sup>

In conclusion, the subunit structure of PglF from *C. jejuni* adopts the classical fold for those members belonging to the SDR superfamily. Strikingly, however, whereas its quaternary structure is dimeric, the manner in which the two subunits arrange themselves is unique. Importantly, the typically conserved tyrosine that plays a key role in the catalytic mechanisms of members of the SDR superfamily is a methionine in PglF. On the basis of both kinetic analyses and site-directed mutagenesis experiments, a catalytic mechanism is proposed for PglF that involves a proton shuttle between the C-4' hydroxyl group of the hexose, the hydroxyl group of Thr 395, and the carboxylate group of Asp 396.

## ■ ASSOCIATED CONTENT

### Accession Codes

X-ray coordinates have been deposited in the Research Collaboratory for Structural Bioinformatics, Rutgers University, New Brunswick, N. J. (Accession Nos. SBJU, SBJV, SBJW, SBJX, and SBJY).

## ■ AUTHOR INFORMATION

### Corresponding Author

\*E-mail: [Hazel\\_Holden@biochem.wisc.edu](mailto:Hazel_Holden@biochem.wisc.edu). Fax: 608-262-1319. Phone: 608-262-4988.

### ORCID

Hazel M. Holden: 0000-0001-6214-3638

### Funding

This research was supported in part by NIH Grant GM115921 (to H.M.H.).

### Notes

The authors declare no competing financial interest.

## ■ ACKNOWLEDGMENTS

A portion of the research described in this paper was performed at Argonne National Laboratory, Structural Biology Center at the Advanced Photon Source (U.S. Department of Energy, Office of Biological and Environmental Research, under Contract DE-AC02-06CH11357). We gratefully acknowledge Dr. Randy Alkire and Dr. Krzysztof Lazarski for assistance during the X-ray data collection at Argonne. We also thank Sonia Leclerc for excellent technical assistance. Finally, we thank the two reviewers for carefully reading the manuscript. Their comments were especially helpful.

## ■ ABBREVIATIONS

HEPES, *N*-2-hydroxyethylpiperazine-*N'*-2-ethanesulfonic acid; HEPPS, *N*-2-hydroxyethylpiperazine-*N'*-3-propanesulfonic acid; HPLC, high-performance liquid chromatography; MES,

2-(*N*-morpholino)ethanesulfonic acid; NAD<sup>+</sup>, nicotinamide adenine dinucleotide (oxidized); NADH, nicotinamide adenine dinucleotide (reduced); NADP<sup>+</sup>, nicotinamide adenine dinucleotide phosphate (oxidized); PCR, polymerase chain reaction; Tris, tris-(hydroxymethyl)aminomethane; UDP, uridine diphosphate; UDP-GlcNAc, uridine diphosphate *N*-acetylglucosamine

## REFERENCES

- (1) Neuberger, A. (1938) Carbohydrates in protein: The carbohydrate component of crystalline egg albumin. *Biochem. J.* 32, 1435–1451.
- (2) Nothaft, H., and Szymanski, C. M. (2010) Protein glycosylation in bacteria: sweeter than ever. *Nat. Rev. Microbiol.* 8, 765–778.
- (3) Nothaft, H., and Szymanski, C. M. (2013) Bacterial protein *N*-glycosylation: new perspectives and applications. *J. Biol. Chem.* 288, 6912–6920.
- (4) Galanis, E. (2007) *Campylobacter* and bacterial gastroenteritis. *CMAJ.* 177, 570–571.
- (5) Szymanski, C. M., Yao, R., Ewing, C. P., Trust, T. J., and Guerry, P. (1999) Evidence for a system of general protein glycosylation in *Campylobacter jejuni*. *Mol. Microbiol.* 32, 1022–1030.
- (6) Scott, N. E., Parker, B. L., Connolly, A. M., Paulech, J., Edwards, A. V., Crossett, B., Falconer, L., Kolarich, D., Djordjevic, S. P., Hojrup, P., Packer, N. H., Larsen, M. R., and Cordwell, S. J. (2011) Simultaneous glycan-peptide characterization using hydrophilic interaction chromatography and parallel fragmentation by CID, higher energy collisional dissociation, and electron transfer dissociation MS applied to the *N*-linked glycoproteome of *Campylobacter jejuni*. *Mol. Cell. Proteomics* 10, M000031-MCP000201.
- (7) Young, N. M., Brisson, J. R., Kelly, J., Watson, D. C., Tessier, L., Lanthier, P. H., Jarrell, H. C., Cadotte, N., St. Michael, F., Aberg, E., and Szymanski, C. M. (2002) Structure of the *N*-linked glycan present on multiple glycoproteins in the Gram-negative bacterium, *Campylobacter jejuni*. *J. Biol. Chem.* 277, 42530–42539.
- (8) Riegert, A. S., Young, N. M., Watson, D. C., Thoden, J. B., and Holden, H. M. (2015) Structure of the external aldimine form of PglE, an aminotransferase required for *N,N'*-diacetylbaucosamine biosynthesis. *Protein Sci.* 24, 1609–1616.
- (9) Rangarajan, E. S., Ruane, K. M., Sulea, T., Watson, D. C., Proteau, A., Leclerc, S., Cygler, M., Matte, A., and Young, N. M. (2008) Structure and active site residues of PglD, an *N*-acetyltransferase from the bacillosamine synthetic pathway required for *N*-glycan synthesis in *Campylobacter jejuni*. *Biochemistry* 47, 1827–1836.
- (10) Olivier, N. B., and Imperiali, B. (2008) Crystal structure and catalytic mechanism of PglD from *Campylobacter jejuni*. *J. Biol. Chem.* 283, 27937–27946.
- (11) Schoenhofen, I. C., McNally, D. J., Vinogradov, E., Whitfield, D., Young, N. M., Dick, S., Wakarchuk, W. W., Brisson, J. R., and Logan, S. M. (2006) Functional characterization of dehydratase/aminotransferase pairs from *Helicobacter* and *Campylobacter*: enzymes distinguishing the pseudaminic acid and bacillosamine biosynthetic pathways. *J. Biol. Chem.* 281, 723–732.
- (12) He, X., and Liu, H. W. (2002) Mechanisms of enzymatic C-O bond cleavages in deoxyhexose biosynthesis. *Curr. Opin. Chem. Biol.* 6, 590–597.
- (13) Kallberg, Y., Oppermann, U., Jornvall, H., and Persson, B. (2002) Short-chain dehydrogenases/reductases (SDRs). *Eur. J. Biochem.* 269, 4409–4417.
- (14) Kallberg, Y., Oppermann, U., Jornvall, H., and Persson, B. (2002) Short-chain dehydrogenase/reductase (SDR) relationships: a large family with eight clusters common to human, animal, and plant genomes. *Protein Sci.* 11, 636–641.
- (15) Oppermann, U., Filling, C., Hult, M., Shafiqat, N., Wu, X., Lindh, M., Shafiqat, J., Nordling, E., Kallberg, Y., Persson, B., and Jornvall, H. (2003) Short-chain dehydrogenases/reductases (SDR): the 2002 update. *Chem.-Biol. Interact.* 143–144, 247–253.
- (16) Kavanagh, K. L., Jornvall, H., Persson, B., and Oppermann, U. (2008) Medium- and short-chain dehydrogenase/reductase gene and protein families: the SDR superfamily: functional and structural diversity within a family of metabolic and regulatory enzymes. *Cell. Mol. Life Sci.* 65, 3895–3906.
- (17) Kallberg, Y., Oppermann, U., and Persson, B. (2010) Classification of the short-chain dehydrogenase/reductase superfamily using hidden Markov models. *FEBS J.* 277, 2375–2386.
- (18) Duax, W. L., Ghosh, D., and Pletnev, V. (2000) Steroid dehydrogenase structures, mechanism of action, and disease. *Vitam. Horm.* 58, 121–148.
- (19) Duax, W. L., Pletnev, V., Addlagatta, A., Bruenn, J., and Weeks, C. M. (2003) Rational proteomics I. Fingerprint identification and cofactor specificity in the short-chain oxidoreductase (SCOR) enzyme family. *Proteins: Struct., Funct., Genet.* 53, 931–943.
- (20) Somoza, J. R., Menon, S., Schmidt, H., Joseph-McCarthy, D., Dessen, A., Stahl, M. L., Somers, W. S., and Sullivan, F. X. (2000) Structural and kinetic analysis of *Escherichia coli* GDP-mannose 4,6 dehydratase provides insights into the enzyme's catalytic mechanism and regulation by GDP-fucose. *Structure* 8, 123–135.
- (21) Allard, S. T., Giraud, M. F., Whitfield, C., Graninger, M., Messner, P., and Naismith, J. H. (2001) The crystal structure of dTDP-D-glucose 4,6-dehydratase (RmlB) from *Salmonella enterica* serovar *Typhimurium*, the second enzyme in the dTDP-L-rhamnose pathway. *J. Mol. Biol.* 307, 283–295.
- (22) Gross, J. W., Hegeman, A. D., Gerratana, B., and Frey, P. A. (2001) Dehydration is catalyzed by glutamate-136 and aspartic acid-135 active site residues in *Escherichia coli* dTDP-glucose 4,6-dehydratase. *Biochemistry* 40, 12497–12504.
- (23) Hegeman, A. D., Gross, J. W., and Frey, P. A. (2001) Probing catalysis by *Escherichia coli* dTDP-glucose-4,6-dehydratase: identification and preliminary characterization of functional amino acid residues at the active site. *Biochemistry* 40, 6598–6610.
- (24) Allard, S. T., Beis, K., Giraud, M. F., Hegeman, A. D., Gross, J. W., Wilmouth, R. C., Whitfield, C., Graninger, M., Messner, P., Allen, A. G., Maskell, D. J., and Naismith, J. H. (2002) Toward a structural understanding of the dehydratase mechanism. *Structure (Oxford, U. K.)* 10, 81–92.
- (25) Hegeman, A. D., Gross, J. W., and Frey, P. A. (2002) Concerted and stepwise dehydration mechanisms observed in wild-type and mutated *Escherichia coli* dTDP-glucose 4,6-dehydratase. *Biochemistry* 41, 2797–2804.
- (26) Mulichak, A. M., Bonin, C. P., Reiter, W. D., and Garavito, R. M. (2002) Structure of the MURI GDP-mannose 4,6-dehydratase from *Arabidopsis thaliana*: implications for ligand binding and specificity. *Biochemistry* 41, 15578–15589.
- (27) Beis, K., Allard, S. T., Hegeman, A. D., Murshudov, G., Philp, D., and Naismith, J. H. (2003) The structure of NADH in the enzyme dTDP-D-glucose dehydratase (RmlB). *J. Am. Chem. Soc.* 125, 11872–11878.
- (28) Allard, S. T., Cleland, W. W., and Holden, H. M. (2004) High resolution X-ray structure of dTDP-glucose 4,6-dehydratase from *Streptomyces venezuelae*. *J. Biol. Chem.* 279, 2211–2220.
- (29) Webb, N. A., Mulichak, A. M., Lam, J. S., Rocchetta, H. L., and Garavito, R. M. (2004) Crystal structure of a tetrameric GDP-D-mannose 4,6-dehydratase from a bacterial GDP-D-rhamnose biosynthetic pathway. *Protein Sci.* 13, 529–539.
- (30) Vogan, E. M., Bellamacina, C., He, X., Liu, H. W., Ringe, D., and Petsko, G. A. (2004) Crystal structure at 1.8 Å resolution of CDP-D-glucose 4,6-dehydratase from *Yersinia pseudotuberculosis*. *Biochemistry* 43, 3057–3067.
- (31) Koropatkin, N. M., and Holden, H. M. (2005) Structure of CDP-D-glucose 4,6-dehydratase from *Salmonella typhi* complexed with CDP-D-xylose. *Acta Crystallogr., Sect. D: Biol. Crystallogr.* 61, 365–373.
- (32) Rosano, C., Zuccotti, S., Sturla, L., Fruscione, F., Tonetti, M., and Bolognesi, M. (2006) Quaternary assembly and crystal structure of GDP-D-mannose 4,6 dehydratase from *Paramecium bursaria* Chlorella virus. *Biochem. Biophys. Res. Commun.* 339, 191–195.

(33) Ishiyama, N., Creuzenet, C., Miller, W. L., Demendi, M., Anderson, E. M., Harauz, G., Lam, J. S., and Berghuis, A. M. (2006) Structural studies of FlaA1 from *Helicobacter pylori* reveal the mechanism for inverting 4,6-dehydratase activity. *J. Biol. Chem.* 281, 24489–24495.

(34) Morrison, J. P., Schoenhofen, I. C., and Tanner, M. E. (2008) Mechanistic studies on PseB of pseudaminic acid biosynthesis: a UDP-N-acetylglucosamine 5-inverting 4,6-dehydratase. *Bioorg. Chem.* 36, 312–320.

(35) Miyafusa, T., Caaveiro, J. M., Tanaka, Y., and Tsumoto, K. (2013) Dynamic elements govern the catalytic activity of CapE, a capsular polysaccharide-synthesizing enzyme from *Staphylococcus aureus*. *FEBS Lett.* 587, 3824–3830.

(36) Miyafusa, T., Caaveiro, J. M., Tanaka, Y., Tanner, M. E., and Tsumoto, K. (2013) Crystal structure of the capsular polysaccharide synthesizing protein CapE of *Staphylococcus aureus*. *Biosci. Rep.* 33, 463–474.

(37) Creuzenet, C., Urbanic, R. V., and Lam, J. S. (2002) Structure-function studies of two novel UDP-GlcNAc C6 dehydratases/C4 reductases. Variation from the SYK dogma. *J. Biol. Chem.* 277, 26769–26778.

(38) McCoy, A. J., Grosse-Kunstleve, R. W., Adams, P. D., Winn, M. D., Storoni, L. C., and Read, R. J. (2007) Phaser crystallographic software. *J. Appl. Crystallogr.* 40, 658–674.

(39) Emsley, P., and Cowtan, K. (2004) Coot: model-building tools for molecular graphics. *Acta Crystallogr., Sect. D: Biol. Crystallogr.* 60, 2126–2132.

(40) Murshudov, G. N., Vagin, A. A., and Dodson, E. J. (1997) Refinement of macromolecular structures by the maximum-likelihood method. *Acta Crystallogr., Sect. D: Biol. Crystallogr.* 53, 240–255.

(41) Otwinowski, Z., and Minor, W. (1997) Processing of X-ray diffraction data collected in oscillation mode. *Methods Enzymol.* 276, 307–326.

(42) Laskowski, R. A., Moss, D. S., and Thornton, J. M. (1993) Main-chain bond lengths and bond angles in protein structures. *J. Mol. Biol.* 231, 1049–1067.

(43) Allard, S. T., Giraud, M. F., and Naismith, J. H. (2001) Epimerases: structure, function and mechanism. *Cell. Mol. Life Sci.* 58, 1650–1665.

(44) Liu, Y., Thoden, J. B., Kim, J., Berger, E., Gulick, A. M., Ruzicka, F. J., Holden, H. M., and Frey, P. A. (1997) Mechanistic roles of tyrosine 149 and serine 124 in UDP-galactose 4-epimerase from *Escherichia coli*. *Biochemistry* 36, 10675–10684.

(45) Thoden, J. B., Wohlers, T. M., Fridovich-Keil, J. L., and Holden, H. M. (2000) Crystallographic evidence for Tyr 157 functioning as the active site base in human UDP-galactose 4-epimerase. *Biochemistry* 39, 5691–5701.

(46) DeLano, W. L. (2002) The PyMOL Molecular Graphics System. DeLano Scientific, San Carlos, CA, USA, *The PyMOL Molecular Graphics System*, DeLano Scientific, San Carlos, CA, USA.